Geophysical Journal International

Geophys. J. Int. (2014) **199,** 1572–1585 doi: 10.1093/gji/ggu358
GJI Seismology

Accurate 3-D finite difference computation of traveltimes in strongly heterogeneous media

M. Noble,[1] A. Gesret[1] and N. Belayouni[1,2]

[1]*Mines ParisTech,PSL - Research University, Centre de Géosciences,* 35 *Rue St Honoré, F-*77300 *Fontainebleau, France.*
E-mail: Mark.Noble@mines-paristech.fr
[2]*Magnitude, Research and Development, Centre de Regain, Route de Marseille, F-*04220 *Sainte-Tulle, France*

Accepted 2014 September 9. Received 2014 September 9; in original form 2014 January 31

SUMMARY

Seismic traveltimes and their spatial derivatives are the basis of many imaging methods such as pre-stack depth migration and tomography. A common approach to compute these quantities is to solve the eikonal equation with a finite-difference scheme. If many recently published algorithms for resolving the eikonal equation do now yield fairly accurate traveltimes for most applications, the spatial derivatives of traveltimes remain very approximate. To address this accuracy issue, we develop a new hybrid eikonal solver that combines a spherical approximation when close to the source and a plane wave approximation when far away. This algorithm reproduces properly the spherical behaviour of wave fronts in the vicinity of the source. We implement a combination of 16 local operators that enables us to handle velocity models with sharp vertical and horizontal velocity contrasts. We associate to these local operators a global fast sweeping method to take into account all possible directions of wave propagation. Our formulation allows us to introduce a variable grid spacing in all three directions of space. We demonstrate the efficiency of this algorithm in terms of computational time and the gain in accuracy of the computed traveltimes and their derivatives on several numerical examples.

Key words: Numerical solutions; Computational seismology; Wave propagation.

1 INTRODUCTION

The finite-difference (FD) approximation to the eikonal equation was first introduced by Vidale (1988, 1990) to propagate first-arrival times in 2-D and 3-D heterogeneous velocity models. eikonal solvers have been used in many seismological problems, and are particularly well adapted to applications that involve very large data sets. The eikonal solver has been used in 3-D refraction/reflection tomography (e.g. Hole 1992; Zelt 1996; Zelt & Barton 1998) and in 2-D and 3-D pre-stack depth migration (Gray & May 1994; Bevc 1997; Marsset *et al.* 1998; Buske 1999a,b). Even today, for seismic exploration applications such as 3-D refraction tomography, this method is still very attractive from a computational point of view (Taillandier *et al.* 2009; Noble *et al.* 2010). The aim of this paper is to propose a fast, robust and accurate eikonal scheme useful for processing very large data sets that are constantly increasing in size.

The original 2-D and 3-D method proposed by Vidale (1988, 1990) based on a FD scheme does produce relatively accurate traveltimes for smooth velocity models. The accuracy of this approach has been thoroughly discussed by Lecomte *et al.* (2000) and Hole & Zelt (1995). In the presence of strong and sharp velocity contrasts, first arrivals are not always guaranteed with Vidale's original method. Podvin & Lecomte (1991) proposed an alternative strategy to be able to handle such heterogeneous models. They proposed different FD operators and they used a physical representation of the slowness model with square cells of constant slowness. With this alternative scheme, they introduced extra operators that enabled to handle properly the head waves, but the computed traveltimes still did exhibit some inaccuracy. To deal with these wave front discontinuities, van Trier & Symes (1991) proposed an alternative scheme based on a first order upwind FD operator. Hole & Zelt (1995) combined Vidale's scheme based only on FD operators with Podvin and Lecomte extra operators that clearly improved accuracy. Afnimar & Koketsu (2000) further improved the resolution of the eikonal by combining all operators of both authors.

Although the algorithms just mentioned previously do yield precise traveltimes for most applications, the spatial derivatives of these traveltimes are not accurate enough to be able to compute reliable auxiliary quantities such as take-off angle and amplitude. To gain in accuray some authors proposed schemes with higher order FD operators (e.g. Popovici & Sethian 2002; Rawlinson & Sambridge 2004a,b). Kim & Cook (1999) developed an eikonal solver based on a essentially non-oscillatory (ENO) FD scheme (Shu & Osher 1988, 1989). The interesting property of ENO is that it can be extended to very high orders of accuracy and remains stable. Buske & Kästner (2004) developed a very

accurate solver in polar coordinates based on the ENO scheme. Qian & Symes (2002) obtained similar accuracy by implementing a Weighted ENO scheme that requires less computational effort and is more stable. To propagate the traveltimes accross the entire grid many authors adopted the expanding square box originally proposed by Vidale (1988) that does not always guarantee first arrivals. An alternative solution to deal with this causality problem is to follow the expanding wave front as proposed by Qin *et al.* (1992) or Cao & Greenhalgh (1994). More recently eikonal solvers based on the fast marching method (FMM) have been developed (Sethian 1996, 1999; Popovici & Sethian 2002) and Rawlinson & Sambridge (2004a,b) have demonstrated the robustness of this algorithm on complex models. A more detailed review on grid-based methods can be found in Rawlinson *et al.* (2007).

The FD operators used to solve the eikonal equation implies a plane wave approximation (Qian & Symes 2002). Close to the source a spherical approximation would be more suitable. This problem was already clearly identified by Vidale (1988) and Podvin & Lecomte (1991). Vidale (1988) proposed a solution in 2-D, unfortunately very difficult to implement in 3-D. To overcome this singularity at the source, Qian & Symes (2002) proposed an adaptive method that reduces inaccuracies, however, the overburden is more algorithmic complexity and extra computational cost. Buske & Kästner (2004) propose an alternative by resolving the equation in polar/spherical coordinates that implies additional overhead related to the interpolation from polar to cartesian coordinates necessary for most applications. A similar approach was used by Alkhalifah & Fomel (2001). Kim & Cook (1999) and Rawlinson & Sambridge (2004a) use local grid refinement in the source neighbourhood. Simpler algorithms based on the factored eikonal equation are able to handle this source singularity (Zhang *et al.* 2005; Fomel *et al.* 2009). Solving the factored eikonal equation better approximates the spherical behaviour of wave fronts close to the source but deteriorates the accuracy of traveltimes far away from the source in strongly heterogeneous media.

The objective of this paper is to present an efficient and simple 3-D eikonal solver that is able to overcome the problem of the source singularity, handle velocity models that exhibit strong vertical and horizontal velocity variations, and use variable grid spacing in all three directions of space. The final goal is not only to generate accurate traveltimes but also accurate derivatives, keeping in mind that the computational cost should be minimum to be able to cope with very large data sets.

To fulfil all these objectives we develop a hybrid algorithm that combines a spherical approximation by solving the factored eikonal equation when close to the source and a plane wave approximation by solving the standard eikonal equation when far away from the source. Like all methods dedicated to solve the eikonal equation, the scheme we propose is a combination of a local scheme and a global scheme to propagate the traveltimes across the entire model. To take into account properly all possible waves (transmitted, diffracted, refracted) for the local scheme, we implement the 16 local operators as suggested by Afnimar & Koketsu (2000). Depending on the distance from the source, these operators are used to solve either the factored or standard eikonal equation. We associate to these local operators a global fast sweeping method (Zhao 2005) to take into account all possible directions of wave propagation.

The paper is organized as follows. We first present the 16 local operators necessary to take into account all kind of waves. We then derive these local operators for plane and spherical wave approximation for a different grid spacing in x, y and z directions. For sake of clarity and simplicity, in the main text we develop in detail only the 3-D operator that to our knowledge has not been published even for a constant grid spacing in all three directions. All other operators are derived in the appendix. We focus essentially on solving the eikonal in 3-D, deriving a 2-D scheme from our 3-D solution is straightforward. After a short description of the global scheme, 2-D and 3-D numerical examples demonstrate the gain in accuracy of computed traveltimes and their derivatives obtained with our hybrid method.

2 LOCAL SCHEME

The eikonal equations, for P and S velocities, are obtained by applying the high-frequency approximation when solving the elastic wave equation. This gives in three dimensions

$$\left(\frac{\partial t}{\partial x}\right)^2+\left(\frac{\partial t}{\partial y}\right)^2+\left(\frac{\partial t}{\partial z}\right)^2=s^2(x,y,z), \tag{1}$$

where t is the traveltime, s is the P or S slowness and x, y and z represent the spatial Cartesian coordinates. Solving eq. (1) by FD operators first implies a discretization of the medium. We choose the same physical representation as Podvin & Lecomte (1991). The slowness model is decomposed into rectangular cells in 2-D or parallelepiped cells in 3-D. The slowness is constant inside each cell and the traveltimes are defined (or computed) at all corners of the cells.

For one direction of propagation, for example for a wave propagating downwards, from west to east, north to south; we propose like Afnimar & Koketsu (2000) 16 different operators for the local scheme (Figs 1 and 2). These operators, described below, enable us to take into account properly all possible waves (transmitted, diffracted and refracted).

(i) In the discrete model, 3-D transmission through the cell is the most frequent process by which energy travels to reach a point. This operator that uses the eight traveltimes defined at the corners of the cell (Fig. 1a) was proposed by Vidale (1990).

(ii) The previous operator is not applicable either if some of the neighbouring points are not known or if different wave fronts converge simultaneously in the current cell. To cope with these situations, we use the three 3-D operators proposed by Afnimar & Koketsu (2000) that are based on five points only (Figs 1b–d). In case of converging wave fronts these operators allow to handle them separately.

(iii) To take into account properly head waves propagating along one of the interfaces of the cell, we use three 2-D Vidale (1988) 4 point operators (Fig. 2a) as proposed by Hole & Zelt (1995).

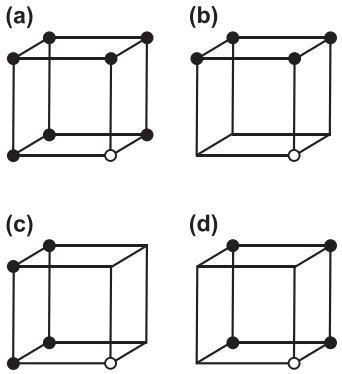

Figure 1. Set of 3-D finite-difference operators for traveltime calculation. The traveltime at the point i, j, k (open circle) is computed using the previously estimated times (black filled circles). (a) One 8 point operator, (b)–(d) three 5 point operators.

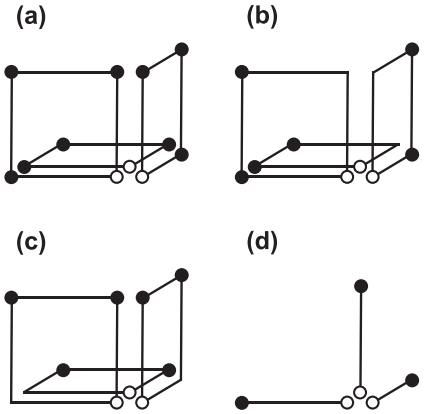

Figure 2. Set of 2-D and 1-D finite-difference operators for traveltime calculation. The traveltime at the point i, j, k (open circle) is computed using the previously estimated times (black filled circles). (a) Three 4 point operators, (b) and (c) six 3 point operators, (d) three 1-D operators.

(iv) As in 3-D, to cope with converging wave fronts or a missing computed traveltime, we also use six 3 point 2-D operators (Figs 2b and c) proposed by Podvin & Lecomte (1991).

(v) And finally we handle head waves propagating along a cell edge with three 1-D operators (Fig. 2d) proposed by Podvin & Lecomte (1991).

In practice, for one direction of propagation, to update the time at the current point we are seeking from its neighbours, we compute the maximum number of the mentioned operators and the smallest traveltime is kept as the correct first-arrival time. The process is repeated through the entire model and for all possible wave propagation directions using the fast sweeping method (described in Section 3). We will now derive the 3-D 8 point operator for the plane and spherical wave approximation for a different grid spacing in x, y and z directions. As mentioned in the introduction, all other operators that are simpler to derive and that can be found in the literature are described in the Appendix.

2.1 3-D plane wave 8 point operator

We first focus on the eight point local operator for the plane wave approximation that is valid when far away from the source. For the derivation of the operator, we first identify traveltimes ($t_{i,j,k}$), slownesses ($s_{i,j,k}$) and the grid spacings (h_i, h_j, h_k) with grid indexes (Fig. 3). The notations might seem heavy but it enables us to derive a general and simple formula valid in 3-D for a different grid spacing in the three directions x, y and z and that is straightforward to implement.

Using the same philosophy as Vidale (1988), the partial derivative with respect to x in eq. (1) can be approximated with FD as

$$\frac{\partial t}{\partial x} \simeq \frac{t_{i,j,k} - t_{i-1,j,k} + t_{i,j-1,k} - t_{i-1,j-1,k} + t_{i,j,k-1} - t_{i-1,j,k-1} + t_{i,j-1,k-1} - t_{i-1,j-1,k-1}}{4h_i}, \tag{2}$$

where $t_{i,j,k}$ is the unknown traveltime we want to estimate and all other seven traveltimes are known. By defining T_i as the sum of these seven traveltimes

$$T_i = t_{i-1,j,k} - t_{i,j-1,k} + t_{i-1,j-1,k} - t_{i,j,k-1} + t_{i-1,j,k-1} - t_{i,j-1,k-1} + t_{i-1,j-1,k-1}, \tag{3}$$

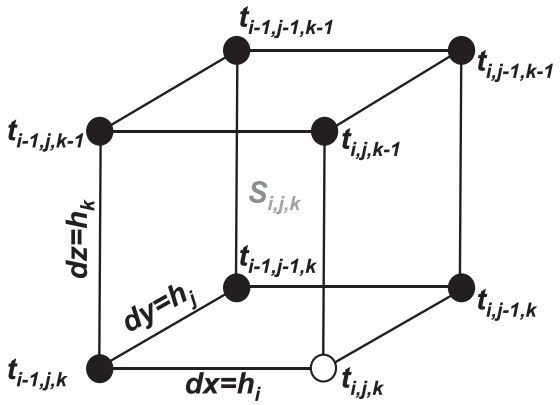

Figure 3. 8 point 3-D finite-difference operator with grid index notation. The traveltime (open circle) is computed using the previously seven estimated times (black filled circles).

eq. (2) simplifies as

$$\frac{\partial t}{\partial x} \simeq \left(\frac{t_{i,j,k} - T_i}{4h_i} \right). \tag{4}$$

Applying the same approach for the y and z directions and after substitution, eq. (1) leads to a very simple second order polynomial to solve

$$\left(\frac{t_{i,j,k} - T_i}{4h_i} \right)^2 + \left(\frac{t_{i,j,k} - T_j}{4h_j} \right)^2 + \left(\frac{t_{i,j,k} - T_k}{4h_k} \right)^2 = s_{i,j,k}^2. \tag{5}$$

Obviously the eq. (5) has two possible roots

$$t_{i,j,k} = \frac{-b \pm \sqrt{b^2 - 4ac}}{2a}, \tag{6}$$

where the coefficients a, b and c are defined as

$$a = \frac{1}{4^{m-1}} \sum_l \frac{1}{h_l^2}, \tag{7}$$

$$b = -\frac{2}{4^{m-1}} \sum_l \frac{T_l}{h_l^2}, \tag{8}$$

$$c = \left(\frac{1}{4^{m-1}} \sum_l \frac{T_l^2}{h_l^2} \right) - s_{i,j,k}^2, \tag{9}$$

where m represents the dimension of space (here $m = 3$) and l the space directions (here $l = i, j, k$).

In order to respect causality when solving eq. (5), we apply the same illumination conditions as proposed by Podvin & Lecomte (1991), this guaranties that the discriminant under the square root is positive. Second, again to insure causality, only the largest root is kept

$$t_{i,j,k} = \frac{-b + \sqrt{b^2 - 4ac}}{2a}. \tag{10}$$

It is worth mentioning that by simply setting $m = 2$ and $l = i, j$, this formulation developed for the 3-D case can be used immediately in 2-D for the three 4 point operators (Fig. 2a). For a constant grid spacing ($h_i = h_j = h$), we find in 2-D exactly the same solution as Vidale (1988). In 3-D our solution is different than the widely used solution proposed by Vidale (1990) that is a truncated formula. Finally, we would like to recall that this 3-D transmission operator is the one that is used the most frequently. This 8 point operator proposed originally by Vidale (1990) is by far the most accurate one we have found. This accuracy relies on the fact that all three partial derivatives are computed at exactly the same position that is the centre of the cell. In this section, we have resolved the standard eikonal equation making locally the assumption of a propagating plane wave. Close to the source, this approximation is not adapted due to strong wave front curvature, in the next section we propose to solve the factored eikonal equation with the same 8 point operator.

2.2 3-D spherical wave 8 point operator

Solving the factored eikonal equation better approximates the spherical behaviour of propagating waves when close to the source. This idea was proposed in 2-D by Fomel *et al.* (2009), we extend the formalism in 3-D, for all the 16 operators and for a different grid spacing. We will now derive in detail the 3-D 8 point operator for the factored eikonal equation, all other operators can be found in the appendix.

We first decompose the traveltime t and the slowness s as

$$t = t_0 \tau, \tag{11}$$

$$s = s_0 \alpha, \tag{12}$$

and t_0 is solution of the eikonal equation for s_0

$$| \bigtriangledown t_0|^2 = s_0^2. \tag{13}$$

If both t_0 and s_0 are known, the resolution of the eikonal equation is equivalent to estimate the perturbation of traveltime τ attributed to the perturbation of the slowness model α. Substituting (11), (12) and (13) in the standard eikonal eq. (1) leads to the factored eikonal equation

$$t_0^2(\bigtriangledown\tau)^2 + \tau^2 s_0^2 + 2\tau t_0 \bigtriangledown t_0 \bigtriangledown \tau = (s_0\alpha)^2. \tag{14}$$

In practice, by setting all cells of s_0 to the value of slowness at the source, we can compute t_0 analytically over the entire grid. The three variables t_0, s_0 and α being known, resolving the factored eikonal eq. (14) amounts to solve a second order polynomial in τ. Once τ is estimated, the time t is simply retrieved by multiplying τ by α.

We use exactly the same philosophy as applied when solving the standard eikonal equation. As for the plane wave approximation, the partial derivatives of τ are approximated using eight neighbouring points. For example, the partial derivative of τ with respect to x is defined using eq. (2) by simply replacing t by τ. As for the plane wave approximation, we sum the seven known perturbations in $\boldsymbol{\tau}_i$, $\boldsymbol{\tau}_j$ and $\boldsymbol{\tau}_k$. After substitution in the factored eikonal eq. (14), we obtain the coefficients a, b and c of the polynomial we want to solve

$$a = \frac{t_0^2}{4^{m-1}} \sum_l \frac{1}{h_l^2} + \frac{t_0}{2^{m-2}} \sum_l \frac{t_{0,l}}{h_l} + s_0^2, \tag{15}$$

$$b = -\frac{2t_0^2}{4^{m-1}} \sum_l \frac{\tau_l}{h_l^2} - \frac{t_0}{2^{m-2}} \sum_l \frac{\tau_l t_{0,l}}{h_l}, \tag{16}$$

$$c = \frac{t_0^2}{4^{m-1}} \sum_l \frac{\boldsymbol{\tau}_l{}^2}{h_l^2} - (s_0\alpha)^2, \tag{17}$$

where m represents the dimension of the grid (here $m = 3$) and l the directions (here $l = i, j, k$). We denoted by t_0 the analytical time and by $t_{0,l}$ its derivative with respect to the l direction at the point i, j, k; by s_0 the initial slowness and by α the perturbation of the initial slowness in the i, j, k cell. Setting $m = 2$ and $l = i, j$, this formulation developed for the 3-D case can be used immediately in 2-D for the three 4 point operators (Fig. 2a).

Close to the source, using the factored eikonal equation greatly improves accuracy compared to a direct numerical solution of the standard eikonal equation. Before illustrating the accuracy of this approximation, we will first briefly describe the global scheme to propagate traveltimes across the entire model.

3 GLOBAL SCHEME

For the local scheme described in the previous section, we developed the different operators for one direction of propagation only: downwards from west to east and north to south. In a 3-D medium there are eight possible propagation directions that should be considered. The formulation of the local operators for the seven other directions is the same, only the indexes of neighbouring points is different depending on direction. In order to propagate the wave fronts over the entire model and take into account all possible directions of propagation, we adopt the fast sweeping method proposed by Zhao (2005). Compared to the propagation schemes proposed by Podvin & Lecomte (1991) and Hole & Zelt (1995) this method has the great advantage of being very simple to implement. For most applications the fast sweeping method turns out to be very efficient in terms of CPU time. For really very heterogeneous velocity models global schemes based on following the expanding wave front (Qin *et al.* 1992; Cao & Greenhalgh 1994; Popovici & Sethian 2002) or the FMM method (Rawlinson & Sambridge 2004a,b) might be more suitable.

Thus, the algorithm we propose to compute first-arrival times of seismic waves in a 3-D model combining our local operators with the fast sweeping approach is summarized as follows:

(i) First assign the traveltime at the source location to $t_{i_{src}, j_{src}, k_{src}} = 0$ and very big values at all other gridpoints $t_{i,j,k} = \infty$.

(ii) Sweep the entire domain ($N_x \times N_y \times N_z$ gridpoints) with eight alternating orderings repeatedly:

(1) $i = 1 : N_x$; $j = 1 : N_y$; $k = 1 : N_z$, (2) $i = N_x : 1$; $j = 1 : N_y$; $k = 1 : N_z$,
(3) $i = 1 : N_x$; $j = N_y : 1$; $k = 1 : N_z$, (4) $i = 1 : N_x$; $j = 1 : N_y$; $k = N_z : 1$,
(5) $i = 1 : N_x$; $j = N_y : 1$; $k = N_z : 1$, (6) $i = N_x : 1$; $j = 1 : N_y$; $k = N_z : 1$,
(7) $i = N_x : 1$; $j = N_y : 1$; $k = 1 : N_z$, (8) $i = N_x : 1$; $j = N_y : 1$; $k = N_z : 1$.

(iii) During the different sweeps, at each gridpoint:

Estimate three traveltimes using the 1-D operators (Fig. 2d),
Estimate three traveltimes using the 2-D operators based on 4 points (Fig. 2a),

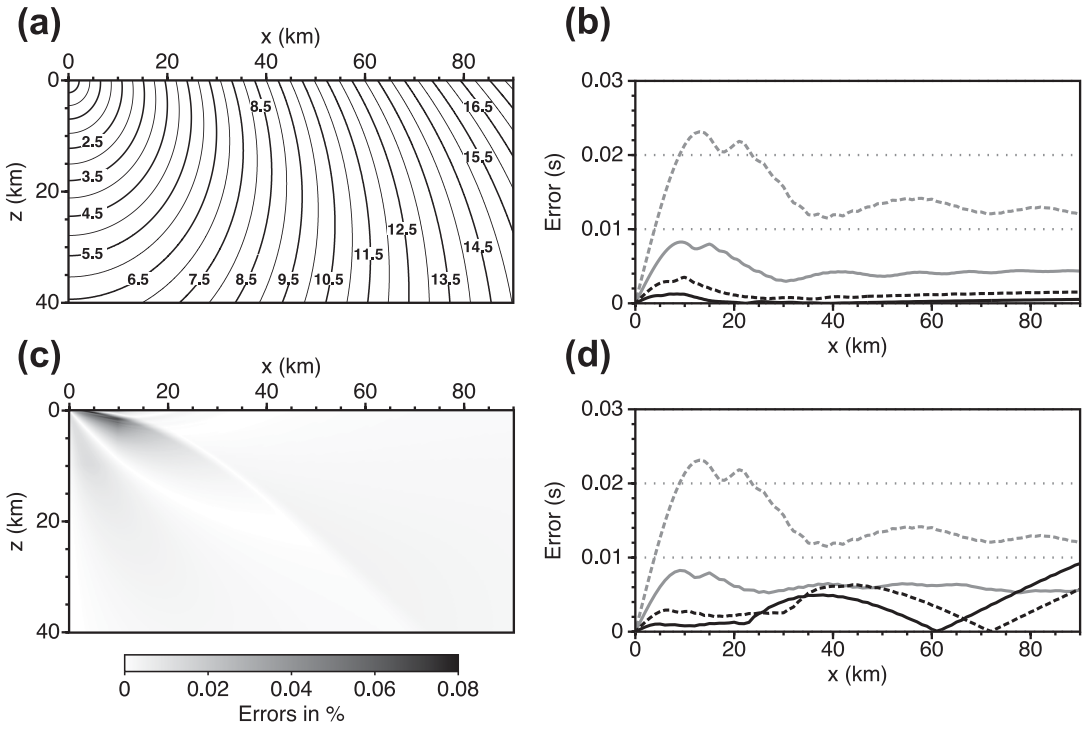

Figure 4. (a) Wave fronts for a source located at the surface propagating through a medium characterized by a vertical gradient of 0.1 s^{-1} and a velocity at the surface of 4.0 km s^{-1}. (b) Plots of the misfit between numerical and analytic solution for decreasing grid spacing: dx = dz = 1000 m (grey dotted line), dx = dz = 500 m (grey solid line), dx = dz = 250 m (black dotted line) and dx = dz = 125 m (black solid line). (c) Relative error in per cent between hydrid eikonal and analytical solution over the entire model for dx = dz = 125 m. (d) Plots of the misfit between numerical and analytic solution for a constant dx = 1000 m and a decreasing grid spacing in z: dz = 1000 m (grey dotted line), dz = 500 m (grey solid line), dz = 250 m (black dotted line) and dz = 125 m (black solid line).

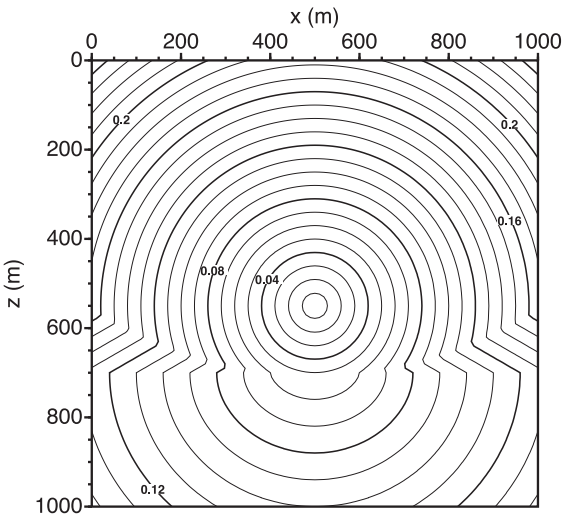

Figure 5. Wave fronts (analytical traveltimes) for a vertical section in the plane of the source that is located at x_{src} = 500 m, y_{src} = 500 m and z_{src} = 550 m, the velocity model is characterized by two layers with a velocity contrast (2:1).

Estimate six traveltimes using the 2-D operators based on 3 points (Figs 2b and c),

Estimate three traveltimes using the 3-D operators based on 5 points (Figs 1b–d),

Estimate one traveltime using the 3-D operator based on 8 points (Fig. 1a).

Finally, for the current point the traveltime is updated by keeping only the lowest value of all the previously estimated times (1-D, 2-D and 3-D operators). In practice, most illumination conditions are usually not verified, so that only a few 2-D and 3-D estimates are actually computed at each point making the algorithm computationally efficient.

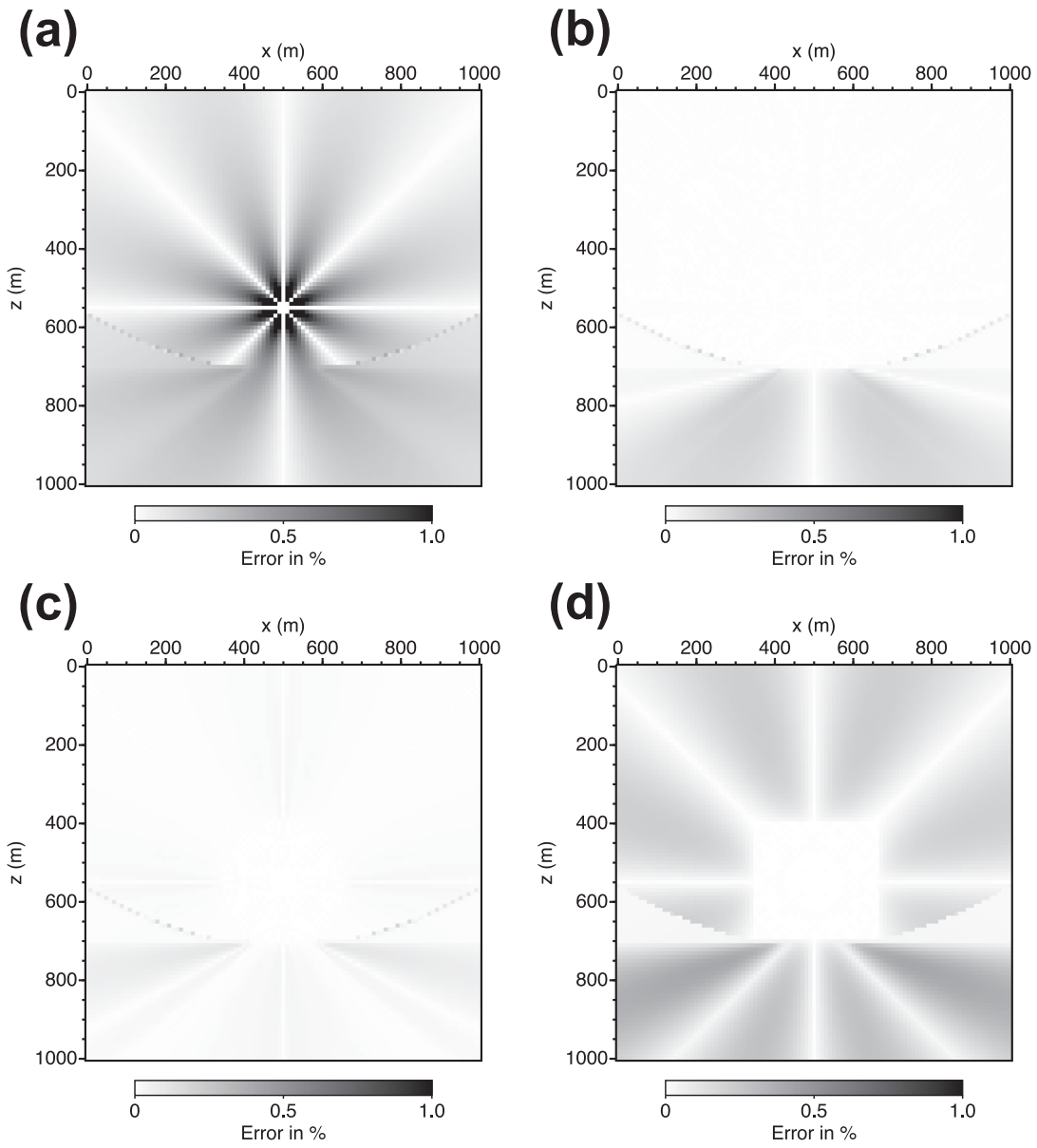

Figure 6. Relative errors in per cent between numerical and analytical solution for the two-layer model (Fig. 5) and for a vertical section in the plane of the source. Numerical traveltimes are computed with plane wave operators only (a), with spherical wave operators only (b), with our hybrid scheme (c) and with the Podvin & Lecomte (1991) algorithm (d).

To ensure accuracy, when close to the source (usually a distance less than 5–10 grid node points away from the source position), 2-D and 3-D traveltimes are estimated using the spherical wave operators (Section 2.2). At greater distance we switch back to the more classical plane wave approximation (Section 2.1). For most realistic velocity models, extending the area where the spherical operators are used does not improve drastically accuracy of computed traveltimes. For velocity models where sharp velocity contrasts are present it is even recommended to switch back to plane operators to ensure accurate computation of refracted traveltimes. This *ad hoc* criterion is similar to the one proposed by Rawlinson & Sambridge (2004b) who adopted a grid refinement strategy. In the following examples, we switch back to plane wave operators at a distance of 10 grid node points horizontally and vertically away from the source.

(iv) Repeat the whole sequence of sweeps until traveltimes remain stable (the number of sweeps obviously depends on the complexity of the velocity model).

The accuracy and computational efficiency of our hybrid algorithm is illustrated on several numerical examples in the next section.

4 NUMERICAL EXAMPLES

The first set of results demonstrates the accuracy of our hybrid eikonal solver in a 2-D medium in which velocity increases linearly with depth. Fig. 4(a) shows wave fronts (analytical traveltimes) for a source located at the surface propagating through the medium that is characterized

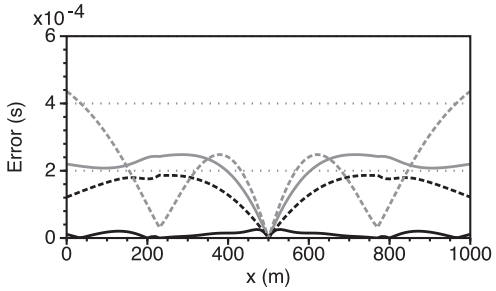

Figure 7. Absolute traveltime errors in the plane of the source for a horizontal profile at $z = 900$ m and $y = 500$ m for plane wave operators (grey solid line), spherical wave operators (black dotted line), hybrid scheme (black solid line) and Podvin & Lecomte (1991) algorithm (grey dotted line).

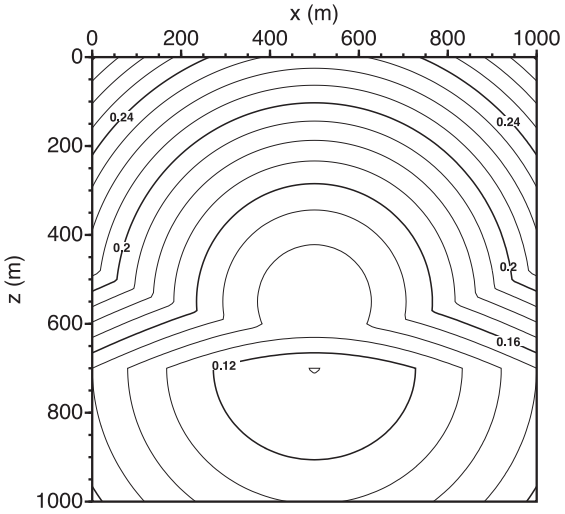

Figure 8. Wave fronts (analytical traveltimes) for a vertical section 400 m out of the plane of the source.

by a vertical velocity gradient of 0.1 s^{-1} and a velocity at the surface of 4.0 km s^{-1}. The model is 90 km × 40 km. The accuracy of our method is illustrated in Fig. 4(b) for four different grid spacings, 1000, 500, 250 and 125 m. In this example grid spacing is the same for both vertical and horizontal directions. Each curve represents the misfit between our numerical solution and analytical traveltimes for receivers located on the surface. For the 1000 m spacing the maximum error is around 20 ms and this error is reduced to less than 1 ms for a spacing of 125 m. Over the entire model Fig. 4(c) shows the relative error between the eikonal and the analytical solution, this error is smaller than 0.08 per cent. This model was used by Rawlinson & Sambridge (2004b) to test their FMM for different FD scheme orders. Despite the fact that our hybrid scheme is only first order we obtain more accurate traveltimes. This improvement is due to a better approximation of the spherical behaviour of wave fronts close to the source. On this specific example Zhang *et al.* (2005) obtained accuracies that are similar to our results. Their celerity domain approach is equivalent to a spherical approximation applied over the entire model. Such an approximation will however deteriorate the accuracy of traveltimes in a strongly heterogeneous medium as we will show for a layered medium example. In Fig. 4(d) each curve represents the misfit between our numerical solution and analytical solution for a constant grid spacing of 1000 m in horizontal direction and with four different grid spacings in the vertical direction, 1000, 500, 250 and 125 m. For this example using a different grid spacing in the horizontal and vertical directions, traveltimes become slightly less accurate but they are still acceptable for most applications. Using a different grid spacing in all directions of space can allow a considerable gain in terms of memory allocation and CPU time, this is particularly useful for 3-D applications. It must be mentioned that if the ratio between the different grid spacing is to high, traveltime errors can increase as illustrated in this example.

The second example illustrates in 3-D the contribution of the different operators in terms of accuracy, and demonstrates that the most precise result is obtained by combining the spherical approximation along with the plane wave one. The velocity model is characterized by two layers with a velocity contrast (2:1), the interface is located at a depth of 700 m. The model is 1000 m × 1000 m × 1000 m with a constant grid spacing of 10 m in all three directions x, y and z. Fig. 5 shows the analytical wave fronts for a vertical section in the plane of the source that is located at $x_{src} = 500$ m, $y_{src} = 500$ m and $z_{src} = 550$ m. For the same vertical section position ($y = 500$ m) Fig. 6(a) shows the relative errors with respect to the analytical solution (in per cent) when computing traveltimes only with the plane wave operators described in the Section 2.1. The strongest errors (around 2 per cent) occur near the source where the plane wave assumption is not adapted, they are drastically reduced (0.2 per cent) when the spherical wave operators described in Section 2.2 are used for traveltime computations (Fig. 6b). Despite a great improvement some inacurracies remain visible below the interface. When using the hybrid scheme that combines spherical approximation when close to the source and plane wave approximation when further away from the source, relative errors over the whole

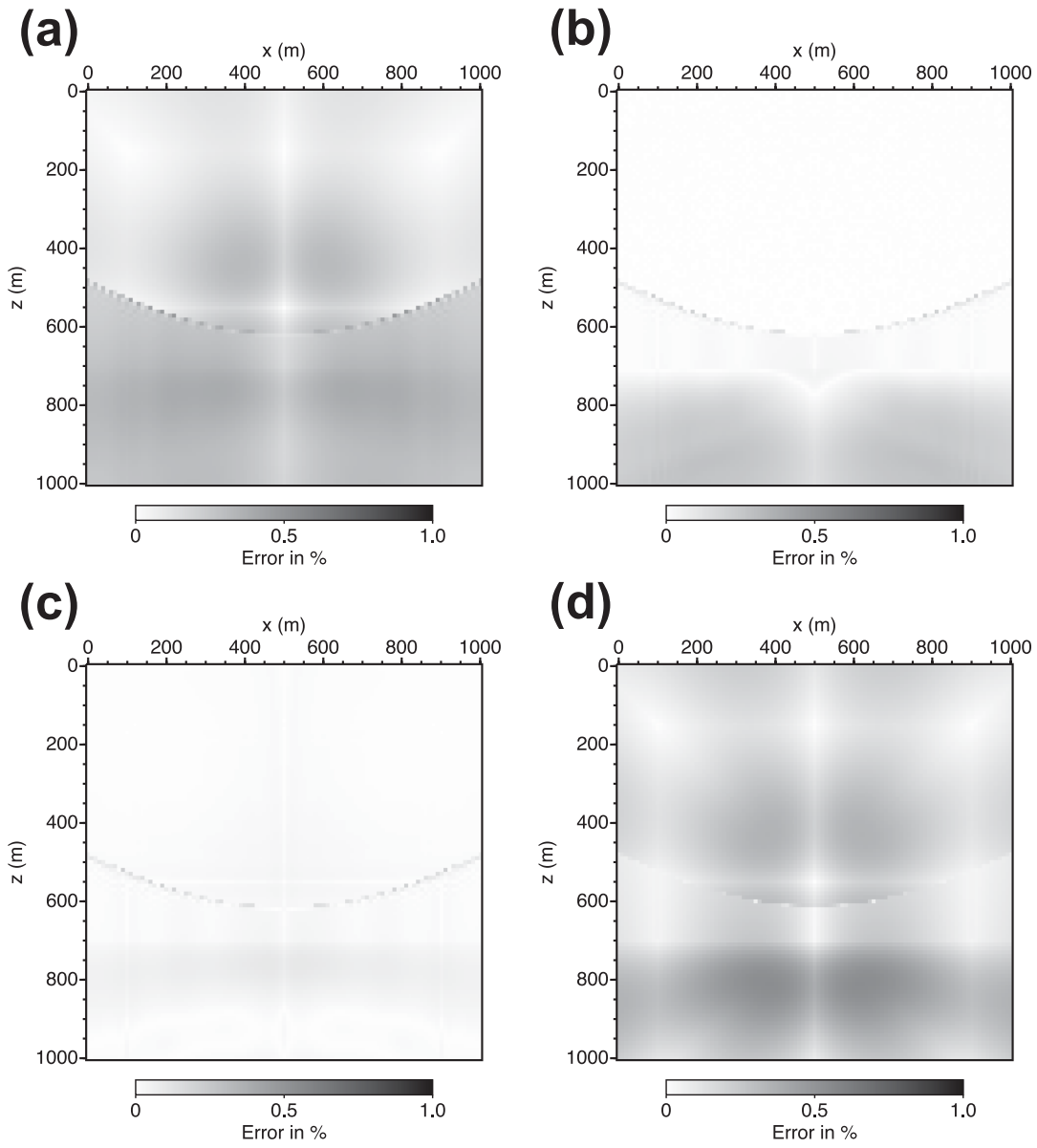

Figure 9. Relative errors for a vertical section 400 m out of the plane of the source. Information is plotted in the same way as Fig. 6.

section are smaller than 0.1 per cent (Fig. 6c). For this example the spherical operators were used within a radius of a 100 m around the source corresponding to 10 gridpoints. As a reference we also display the relative errors obtained with the widely used algorithm developed by Podvin & Lecomte (1991), maximum errors are around 0.4 per cent (Fig. 6d). To summarize the improvement when using our hybrid algorithm, Fig. 7 shows for the same four different schemes (plane wave, spherical wave, hybrid scheme and Podvin algorithm) the absolute traveltime errors for a horizontal profile at a depth of 900 m and $y = 500$ m. The maximum error of our approach is around 2.5×10^{-5} s.

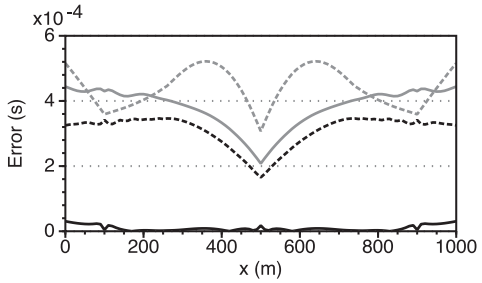

Figure 10. Absolute traveltime errors for a vertical section 400 m out of the plane of the source. Information is plotted in the same way as Fig. 7.

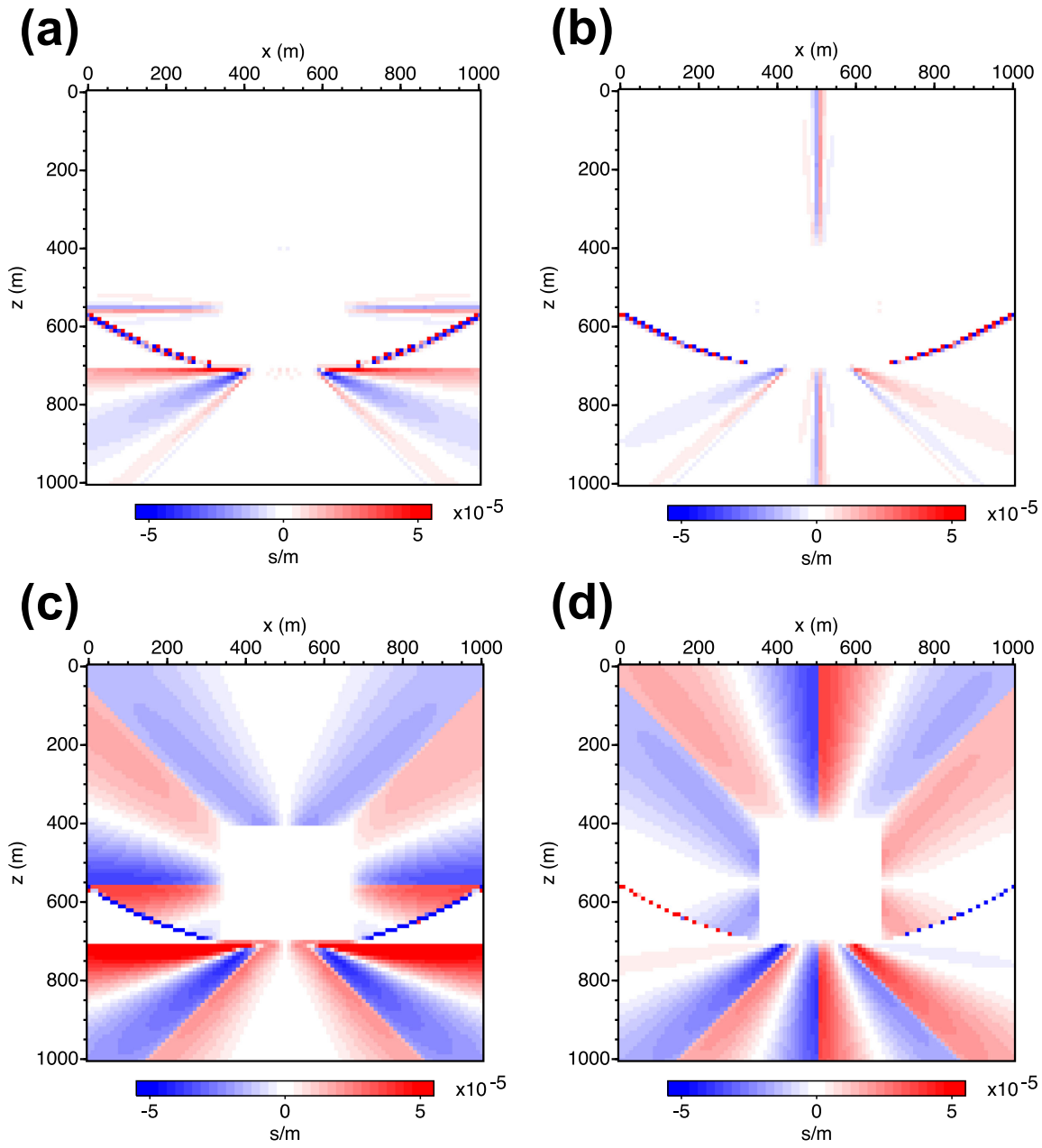

Figure 11. Accuracy of spatial derivatives of traveltimes. Errors between hybrid scheme and analytical solution with respect to Z (a) and with respect to X (b). Errors between Podvin & Lecomte (1991) scheme and analytical solution with respect to Z (c) and with respect to X (d).

We did the same error analysis for a vertical section 400 m out of the plane of the source (Figs 8–10). For our plane wave operator scheme (Fig. 9a) errors decrease considerably (0.4 per cent), this is expected as the plane wave approximation better approximates the behaviour of wave fronts when far from the source. On the contrary traveltime accuracy deteriorates for the spherical approximation (0.3 per cent) particularly below the interface (Fig. 9b), while accuracy remains the same (0.1 per cent) for our hybrid scheme (Fig. 9c). Errors for the Podvin algorithm (Fig. 9d) tend to increase over the entire section and reach a maximum of 0.55 per cent. Fig. 10 shows that our hybrid scheme enables us to gain one order of magnitude in terms of traveltime accuracy.

To complete this analysis, we illustrate the gain in accuracy of the spatial derivatives of the traveltimes on the same velocity model. Figs 11(a) and (b) show the derivative errors between our hybrid scheme and the analytical solution for a vertical section in the plane of the source. As a comparison Figs 11(c) and (d) represent the errors for the Podvin & Lecomte (1991) scheme. Once again, over the entire section, our proposed eikonal solver produces more reliable results.

We finally illustrate the computation of the traveltimes in a more realistic 3-D velocity model (Fig. 12a) that is inspired from the SEG/EAGE Overthrust model. The overall model size is 20 km $\times$ 20 km $\times$ 2.2 km with a grid spacing of dx = 25 m, dy = 25 m and dz = 25 m. For this 800 $\times$ 800 $\times$ 160 cell model two global sweeps were necessary to obtain accurate traveltimes. On an Intel i7 3.2 GHz

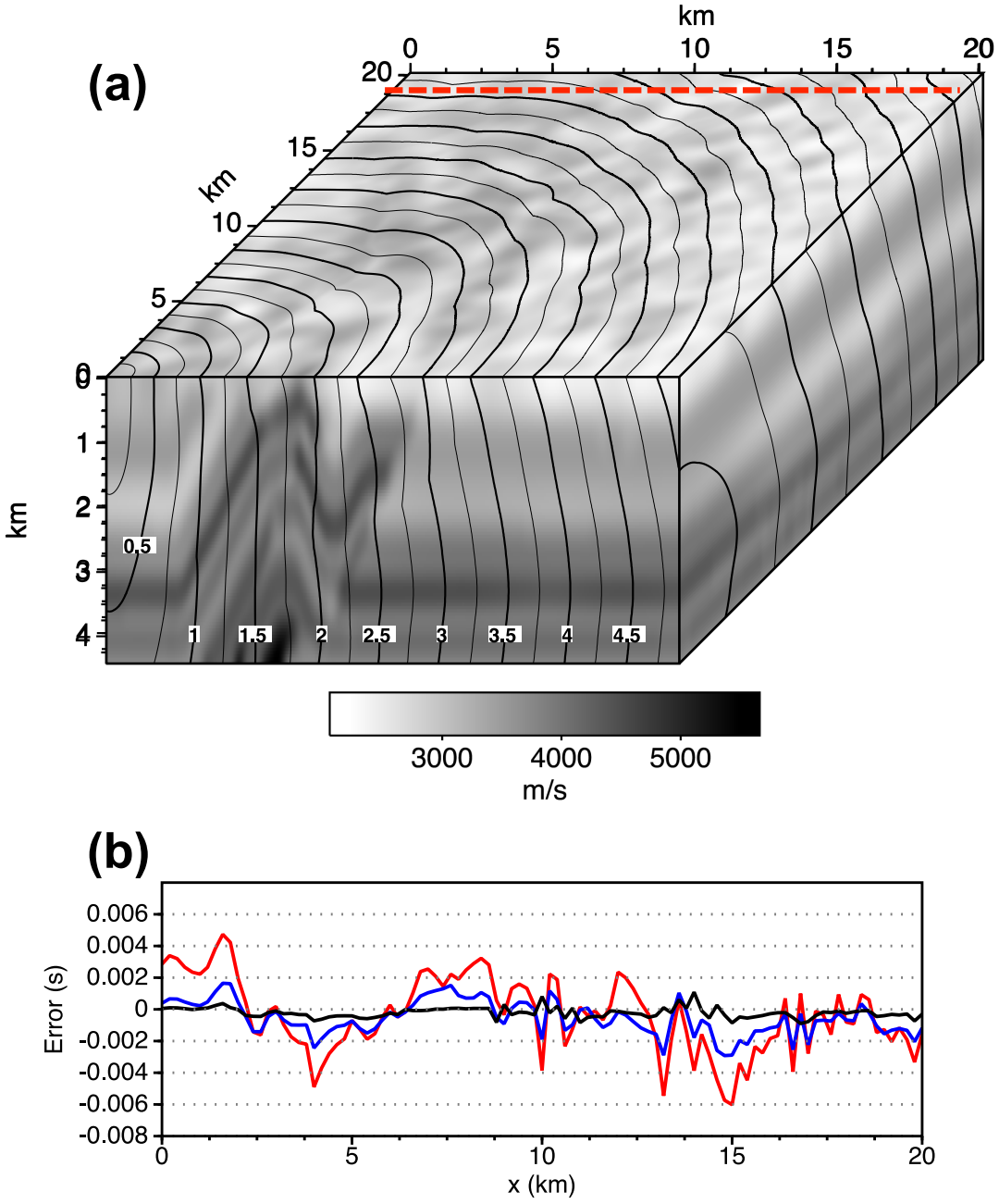

Figure 12. (a) 3-D velocity model inspired form the SEG/EAGE Overthrust model and traveltimes computed with our hybrid scheme. The model size is 20 km × 20 km × 4.4 km with a grid spacing of dx = 25 m, dy = 25 m and dz = 25 m. (b) Error plots for grid spacings of 200 m (red), 100 m (blue) and 50 m (black) for a line of receivers at a distance of 19 km away form the source. Position of receivers is marked in Fig. 12(a).

processor, 40 s of CPU time were required to compute the traveltimes. The CPU time of the algorithm is strictly proportional to the number of nodes in the velocity model, as a reference calculating the traveltimes in a 100 × 100 × 100 cell model takes 0.4 s. To finally validate the convergence of our algorithm, for this heterogenous model, we took as a reference the traveltimes computed with a grid spacing of 25 m in all three directions. Fig. 12(b) shows the error plots for grid spacings of 200, 100 and 50 m for a line of receivers at a distance of 19 km away form the source. Position of receivers is marked in Fig. 12(a). The error being the difference between the traveltimes computed in the coarse grid and the reference traveltimes. As grid spacing decreases traveltimes converge to the reference solution.

5 CONCLUSION

We have presented a new 2-D and 3-D hybrid eikonal solver that combines a spherical approximation when close to the source and a plane wave approximation when far away. This algorithm handles properly the spherical behaviour of wave fronts in the vicinity of the source and does not need any specific initialization as required by most algorithms. We implemented 16 local operators to take into account all possible

waves (transmitted, diffracted, refracted) and to cope with velocity models that exhibit strong vertical and horizontal velocity variations. Our formulation enables us to introduce a variable grid spacing in all three directions of space, this feature can be very useful for non-standard acquisition geometries and/or to represent properly small spatial velocity variations that could require a finer grid spacing in one direction only (depth for example). Associated to the local operators we implemented a global fast sweeping method to take into account all possible directions of wave propagation. 2-D and 3-D numerical examples (for continuous media and for sharp velocity contrast models) not only demonstrate the gain in accuracy of the computed traveltimes but also of their derivatives. These accurate derivatives are necessary if one wants to compute auxiliary quantities such as take-off angles and amplitudes.

ACKNOWLEDGEMENTS

The authors would particularly like to thank Pascal Podvin, MINES ParisTech for many fruitful discussions concerning eikonal solvers. We thank Nick Rawlinson and an anonymous reviewer for their valuable comments and suggestions for the improvement of the manuscript.

REFERENCES

Afnimar & Koketsu, K., 2000. Finite difference traveltime calculation for head waves travelling along an irregular interface, *Geophys. J. Int.,* **143,** 729–734.

Alkhalifah, T. & Fomel, S., 2001. Implementing the fast marching eikonal solver: spherical versus Cartesian coordinates, *Geophys. Prospect.,* **49,** 165–178.

Bevc, D., 1997. Imaging complex structures with semirecursive Kirchhoff migration, *Geophysics,* **62,** 577–588.

Buske, S., 1999a. 3-D prestack Kirchhoff migration of the ISO89-3D data set, *Pure appl. Geophys.,* **156,** 151–171.

Buske, S., 1999b. Three-dimensional pre-stack Kirchhoff migration of deep seismic reflection data, *Geophys. J. Int.,* **137,** 1243–1260.

Buske, S. & Kästner, U., 2004. Efficient and accurate computation od seismic traveltimes and amplitudes, *Geophys. Prospect.,* **52,** 313–322.

Cao, S. & Greenhalgh, S., 1994. Finite-difference solution of the eikonal equation using an efficient, first-arrival, wavefront tracking scheme, *Geophysics,* **59,** 632–643.

Fomel, S., Luo, S. & Zhao, H., 2009. Fast sweeping method for the factored eikonal equation, *J. Comput. Phys.,* **228,** 6440–6455.

Gray, S.H. & May, W.P., 1994. Kirchhoff migration using eikonal equation traveltimes, *Geophysics,* **59,** 810–817.

Hole, J.A., 1992. Nonlinear high-resolution three-dimensional travel-time tomography, *J. geophys. Res.,* **97,** 6553–6562.

Hole, J.A. & Zelt, B.C., 1995. 3-D finite-difference reflection traveltimes, *Geophys. J. Int.,* **121,** 427–434.

Kim, S. & Cook, R., 1999. 3D traveltime computation using second-order ENO scheme, *Geophysics,* **64,** 1867–1876.

Lecomte, I., Gjøystdal, H., Dahle, A. & Pedersen, O.C., 2000. Improving modelling and inversion in refraction seismics with a first-order Eikonal solver, *Geophys. Prospect.,* **48,** 437–454.

Marsset, B., Missiaen, T., De Roeck, Y.H., Noble, M., Versteeg, W. & Henriet, J.P., 1998. Very high resolution 3D marine seismic data processing for geotechnical applications, *Geophys. Prospect.,* **46**(2), 105–120.

Noble, M., Thierry, P., Taillandier, C. & Calandra, H., 2010. High-performance 3D first-arrival traveltime tomography, *Leading Edge,* **29**(1), 86–93.

Podvin, P. & Lecomte, I., 1991. Finite difference computation of traveltimes in very contrasted velocity models: a massively parallel approach and its associated tools, *Geophys. J. Int.,* **105,** 271–284.

Popovici, A.M. & Sethian, J.A., 2002. 3-D imaging using higher order fast marching traveltimes, *Geophysics,* **67,** 604–609.

Qian, J. & Symes, W.W., 2002. An adaptive finite-difference method for traveltimes and amplitudes, *Geophysics,* **67,** 167–176.

Qin, F., Luo, Y., Olsen, K.B., Cai, W. & Schuster, G.T., 1992. Finite-difference solution of the eikonal equation along expanding wavefronts, *Geophysics,* **57,** 478–487.

Rawlinson, N. & Sambridge, M., 2004a. Multiple reflection and transmission phases in complex layered media using a multistage fast marching method, *Geophysics,* **69,** 1338–1350.

Rawlinson, N. & Sambridge, M., 2004b. Wave front evolution in strongly heterogeneous layered media using the fast marching method, *Geophys. J. Int.,* **156,** 631–647.

Rawlinson, N., Hauser, J. & Sambridge, M., 2007. Seismic ray tracing and wavefront tracking in laterally heterogeneous media, *Adv. Geophys.,* **49,** 203–267.

Sethian, J.A., 1996. A fast marching level set method for monotonically advancing fronts, *Proc. Natl. Acad. Sci.,* **93,** 1591–1595.

Sethian, J.A., 1999. *Level Set Methods and Fast Marching Methods,* Cambridge Univ. Press.

Shu, C.-W. & Osher, S., 1988. Efficient implementation of essentially non-oscillatory shock-capturing schemes, *J. Computat. Phys.,* **77,** 439–471.

Shu, C.-W. & Osher, S., 1989. Efficient implementation of essentially non-oscillatory shock-capturing schemes, II, *J. Comput. Phys.,* **83,** 32–78.

Taillandier, C., Noble, M., Chauris, H. & Calandra, H., 2009. First-arrival traveltime tomography based on the adjoint-state method, *Geophysics,* **74**(6), WCB1–WCB10.

van Trier, J. & Symes, W.W., 1991. Upwind finite-difference calculation of traveltimes, *Geophysics,* **56,** 812–821.

Vidale, J., 1988. Finite-difference calculation of travel times, *Bull. seism. Soc. Am.,* **78,** 2062–2076.

Vidale, J., 1990. Finite-difference calculation of travel times in three dimensions, *Geophysics,* **55,** 521–526.

Zelt, C.A., 1996. Seismic velocity structure of the central Chilean margin near the subducting Juan Fernandez ridge: effective inversion of traveltime data across complex, laterally varying structure, in *Proceedings of the 7th Int. Symp., Deep Seismic Profiling of the Continents,* Asilomar, CA (Abstracts).

Zelt, C.A. & Barton, P.J., 1998. Three-dimensional seismic refraction tomography: a comparison of two methods applied to data from the Faeroe Basin, *J. geophys. Res.,* **103,** 7187–7210.

Zhang, L., Rector, J.W. III & Hoversten, G.M., 2005. Eikonal solver in the celerity domain, *Geophys. J. Int.,* **162,** 1–8.

Zhao, H., 2005. A fast sweeping method for Eikonal equations, *Math. Comp.,* **74,** 603–627.

APPENDIX A: 3-D LOCAL COMPUTATIONS

A1 5 point operator

This 5 point operator needs previously estimated traveltimes or perturbations at four gridpoints defining a cell side, which is non adjacent to the point i, j, k (Figs 1b–d). We here consider the wave transmitted from the left side of the cell towards the point i, j, k (Fig. 1c). Equivalent equations can be easily derived for the wave transmitted from the top side (Fig. 1b) or from the back side (Fig. 1d).

A1.1 Plane wave operator

For the plane wave approximation, the partial derivatives of the traveltime can be approximated with finite-differences as (see Fig. 3 for grid index notations)

$$\frac{\partial t}{\partial x} \simeq \frac{t_{i,j,k} - t_{i-1,j,k}}{h_i}, \tag{A1}$$

$$\frac{\partial t}{\partial y} \simeq \frac{t_{i-1,j,k} - t_{i-1,j-1,k} + t_{i-1,j,k-1} - t_{i-1,j-1,k-1}}{2h_j} = \frac{T_j}{2h_j}, \tag{A2}$$

$$\frac{\partial t}{\partial z} \simeq \frac{t_{i-1,j,k} - t_{i-1,j,k-1} + t_{i-1,j-1,k} - t_{i-1,j-1,k-1}}{2h_k} = \frac{T_k}{2h_k}. \tag{A3}$$

Replacing these partial derivatives in the eikonal eq. (1) leads to the traveltime solution

$$t_{i,j,k} = t_{i-1,j,k} + \sqrt{h_i^2 \left[s_{i,j,k}^2 - \left(\frac{T_j}{2h_j}\right)^2 - \left(\frac{T_k}{2h_k}\right)^2 \right]}. \tag{A4}$$

A1.2 Spherical wave operator

For the spherical wave approximation, the partial derivatives of the traveltime perturbation are discretized as for the plane wave approximation by replacing t by τ. We also substitute some terms of these equations in $\boldsymbol{\tau_j}$ and $\boldsymbol{\tau_k}$ and integrate them into the factored eikonal eq. (14). The traveltime perturbation $\tau_{i,j,k}$ solution of the factored eikonal equation is then given by eq. (10) for the following parameters a, b and c

$$a = \frac{t_0^2}{h_i^2} + s_0^2 + \frac{2t_0 t_{0,i}}{h_i}, \tag{A5}$$

$$b = -2t_0 \left(\frac{t_0 \tau_{i-1,j,k}}{h_i^2} + \frac{\tau_{i-1,j,k} t_{0,i}}{h_i} - \frac{\boldsymbol{\tau_j}}{2h_j} t_{0,j} - \frac{\boldsymbol{\tau_k}}{2h_k} t_{0,k} \right), \tag{A6}$$

$$c = t_0^2 \left[\frac{\tau_{i-1,j,k}^2}{h_i^2} + \left(\frac{\boldsymbol{\tau_j}}{2h_j}\right)^2 + \left(\frac{\boldsymbol{\tau_k}}{2h_k}\right)^2 \right] - (s_0\alpha)^2, \tag{A7}$$

with the same notations as described in Section 2.2.

A2 4 point operator

These 4 point operators are used to represent the head waves propagating along one of the three cell sides adjacent to the point i, j, k (Fig. 2a). The solutions are equivalent to those developed in Sections 2.1 and 2.2 for the 8 point operator.

A2.1 Plane wave operator

For the plane wave approximation and for a head wave propagating along the front side, the partial derivatives of traveltime are discretized (see Fig. 3 for grid index notations)

$$\frac{\partial t}{\partial x} \simeq \frac{t_{i,j,k} - t_{i-1,j,k} + t_{i,j,k-1} - t_{i-1,j,k-1}}{2h_i}, \tag{A8}$$

$$\frac{\partial t}{\partial z} \simeq \frac{t_{i,j,k} - t_{i,j,k-1} + t_{i-1,j,k} - t_{i-1,j,k-1}}{2h_k}. \tag{A9}$$

As for the 3-D case (Section 2.1), we pose $T_i = t_{i-1,j,k} - t_{i,j,k-1} + t_{i-1,j,k-1}$ and $T_k = t_{i,j,k-1} - t_{i-1,j,k} + t_{i-1,j,k-1}$. If m represents the dimension of the grid (here $m = 2$) and l the directions (here $l = i, k$), the traveltime solution $t_{i,j,k}$ of the eikonal eq. (1) is given by eq. (10) with a, b and c defined in eqs (7)–(9). The only additive requirement is to select the smaller slowness between the two cells bordering the interface. For example, for the head wave travelling along the front side, $s_{i,j,k}$ in eq. (9) is replaced by $\min(s_{i,j,k}, s_{i,j+1,k})$. We do not derive here the equations for the head waves travelling along the right side and along the bottom side since their traveltimes are computed by simply modifying the indexes defining the directions.

A2.2 Spherical wave operator

In the same way, for the spherical wave 4 point operator, the perturbation of traveltime $\tau_{i,j,k}$ is solution of eq. (10) with a, b and c defined in eqs (15)–(17) by setting $m = 2$ and $l = i, k$. $s_0\alpha$ in eq. (17) is simply replaced by $\min(s_0\alpha_{i,j,k}, s_0\alpha_{i,j+1,k})$.

A3 3 point operator

To cope with converging wave fronts or missing computed traveltime, we also use six 3 point operators (Figs 2b and c) proposed by Podvin & Lecomte (1991).

A3.1 Plane wave operator

For the head wave propagating along the front side from the left interface towards the point i, j, k (Fig. 2b), the partial derivatives are discretized (see Fig. 3 for grid index notations)

$$\frac{\partial t}{\partial x} \simeq \frac{t_{i,j,k} - t_{i-1,j,k}}{h_i}, \tag{A10}$$

$$\frac{\partial t}{\partial z} \simeq \frac{t_{i-1,j,k} - t_{i-1,j,k-1}}{h_k}. \tag{A11}$$

Replacing in the eikonal eq. (1) leads to

$$t_{i,j,k} = t_{i-1,j,k} + \sqrt{h_i^2 \left[\min(s_{i,j,k}, s_{i,j+1,k})^2 - \frac{(t_{i-1,j,k} - t_{i-1,j,k-1})^2}{h_k^2} \right]}. \tag{A12}$$

For the head wave propagating along the front side from the top interface towards the point i, j, k (Fig. 2c), the traveltime solution of the eikonal eq. (1) is

$$t_{i,j,k} = t_{i,j,k-1} + \sqrt{h_k^2 \left[\min(s_{i,j,k}, s_{i,j+1,k})^2 - \frac{(t_{i,j,k-1} - t_{i-1,j,k-1})^2}{h_i^2} \right]}. \tag{A13}$$

If we develop the solution for a constant step ($h_i = h_k = h$), we retrieve the solution proposed by Podvin & Lecomte (1991).

A3.2 Spherical wave operator

For the spherical wave 3 point operator, the partial derivatives are expressed as for the plane wave approximation by replacing t by τ. For the head wave propagating along the front side from the left interface towards the point i, j, k (Fig. 2b), the traveltime perturbation $\tau_{i,j,k}$ solution of the factored eikonal eq. (14) is given by eq. (10) with the following parameters

$$a = \frac{t_0^2}{h_i^2} + s_0^2 + \frac{2 t_0 t_{0,i}}{h_i}, \tag{A14}$$

$$b = -2 t_0 \left(\frac{t_0 \tau_{i-1,j,k}}{h_i^2} + \frac{\tau_{i-1,j,k} t_{0,i}}{h_i} - \frac{\tau_{i-1,j,k} - \tau_{i-1,j,k-1}}{h_k} t_{0,k} \right), \tag{A15}$$

$$c = t_0^2 \left[\frac{\tau_{i-1,j,k}^2}{h_i^2} + \frac{(\tau_{i-1,j,k} - \tau_{i-1,j,k-1})^2}{h_k^2} \right] - [\min(s_0 \alpha_{i,j,k}, s_0 \alpha_{i,j+1,k})]^2. \tag{A16}$$

For the head wave propagating along the front side from the top interface towards the point i, j, k (Fig. 2c), the a, b and c parameters are obtained by simply interchanging i and k in the three above equations.

A4 1-D operator

The traveltime solutions of the three head waves (Fig. 2d) write

$$t_{i,j,k} = t_{i-1,j,k} + h_i \times \min(s_{i,j,k}, s_{i,j+1,k}, s_{i,j,k+1}, s_{i,j+1,k+1}), \tag{A17}$$

$$t_{i,j,k} = t_{i,j-1,k} + h_j \times \min(s_{i,j,k}, s_{i+1,j,k}, s_{i,j,k+1}, s_{i+1,j,k+1}), \tag{A18}$$

$$t_{i,j,k} = t_{i,j,k-1} + h_k \times \min(s_{i,j,k}, s_{i+1,j,k}, s_{i,j+1,k}, s_{i+1,j+1,k}). \tag{A19}$$